AFRL-RX-WP-TP-2012-0278

LOAD-DIFFERENTIAL IMAGING FOR DETECTION AND LOCALIZATION OF FATIGUE CRACKS USING LAMB WAVES (PREPRINT)

X. Chen, J.E. Michaels, S.J. Lee, and T.E. Michaels
Georgia Tech Research Group.

MARCH 2012

Approved for public release; distribution unlimited.
See additional restrictions described on inside pages

STINFO COPY

AIR FORCE RESEARCH LABORATORY
MATERIALS AND MANUFACTURING DIRECTORATE
WRIGHT-PATTERSON AIR FORCE BASE, OH 45433-7750
AIR FORCE MATERIEL COMMAND
UNITED STATES AIR FORCE

REPORT DOCUMENTATION PAGE

Form Approved
OMB No. 0704-0188

The public reporting burden for this collection of information is estimated to average 1 hour per response, including the time for reviewing instructions, searching existing data sources, searching existing data sources, gathering and maintaining the data needed, and completing and reviewing the collection of information. Send comments regarding this burden estimate or any other aspect of this collection of information, including suggestions for reducing this burden, to Department of Defense, Washington Headquarters Services, Directorate for Information Operations and Reports (0704-0188), 1215 Jefferson Davis Highway, Suite 1204, Arlington, VA 22202-4302. Respondents should be aware that notwithstanding any other provision of law, no person shall be subject to any penalty for failing to comply with a collection of information if it does not display a currently valid OMB control number. **PLEASE DO NOT RETURN YOUR FORM TO THE ABOVE ADDRESS**.

1. REPORT DATE *(DD-MM-YY)*	2. REPORT TYPE	3. DATES COVERED *(From - To)*
March 2012	Journal Article	1 March 2012 – 1 March 2012

4. TITLE AND SUBTITLE
LOAD-DIFFERENTIAL IMAGING FOR DETECTION AND LOCALIZATION OF FATIGUE CRACKS USING LAMB WAVES (PREPRINT)

5a. CONTRACT NUMBER
FA8650-09-C-5206

5b. GRANT NUMBER

5c. PROGRAM ELEMENT NUMBER
62102F

6. AUTHOR(S)
X. Chen, J.E. Michaels, S.J. Lee, and T.E. Michaels

5d. PROJECT NUMBER
4349

5e. TASK NUMBER
41

5f. WORK UNIT NUMBER
LP106300

7. PERFORMING ORGANIZATION NAME(S) AND ADDRESS(ES)
Georgia Tech Research Group
505 10th NW
Atlanta, GA 30332-0001

8. PERFORMING ORGANIZATION REPORT NUMBER
AFRL-RX-WP-TP-2012-0278

9. SPONSORING/MONITORING AGENCY NAME(S) AND ADDRESS(ES)
Air Force Research Laboratory
Materials and Manufacturing Directorate
Wright-Patterson Air Force Base, OH 45433-7750
Air Force Materiel Command
United States Air Force

10. SPONSORING/MONITORING AGENCY ACRONYM(S)
AFRL/RXLP

11. SPONSORING/MONITORING AGENCY REPORT NUMBER(S)
AFRL-RX-WP-TP-2012-0278

12. DISTRIBUTION/AVAILABILITY STATEMENT
Approved for public release; distribution unlimited.

13. SUPPLEMENTARY NOTES
The U.S. Government is joint author of this work and has the right to use, modify, reproduce, release, perform, display, or disclose the work. PA Case Number and clearance date: 88ABW-2012-0267, 17 Jan 2012. Preprint journal article to be submitted to NDT & E. This document contains color.

14. ABSTRACT
Fatigue cracks are common and potentially critical defects in metallic plate-like structures, and ultrasonic guided wave methods provide an efficient and relatively low-cost means of crack detection and monitoring. However, widely used baseline subtraction methods may fail under mismatched environmental and operational conditions. In particular, varying applied loads change not only the contact state of a crack but also specimen dimensions and wave speeds, which affect the ultrasonic signal response. The load dependence of crack opening provides a possibility for enhanced crack detection, which is well-known for higher frequency bulk waves. A load-differential method is proposed in this paper whereby guided wave signals obtained at different loads under the same damage state are compared without utilizing previously recorded damage-free data. To demonstrate this method, a fatigue test was performed on an aluminum plate specimen instrumented with a sparse array of piezoelectric transducers. Signal changes due to crack opening effects caused by increasing tensile loads are visualized using delay-and-sum imaging.

15. SUBJECT TERMS
Guided Wave, Sparse Array, Load-differential Imaging, Crack Detection

16. SECURITY CLASSIFICATION OF:			17. LIMITATION OF ABSTRACT:	NUMBER OF PAGES	19a. NAME OF RESPONSIBLE PERSON (Monitor)
a. REPORT	b. ABSTRACT	c. THIS PAGE			Charles Buynak
Unclassified	Unclassified	Unclassified	SAR	24	19b. TELEPHONE NUMBER *(Include Area Code)* N/A

Load-Differential Imaging for Detection and Localization of Fatigue Cracks Using Lamb Waves

Xin Chen, Jennifer E. Michaels, Sang Jun Lee, and Thomas E. Michaels

School of Electrical and Computer Engineering, Georgia Institute of Technology, Atlanta, GA, USA 30332-0250

ABSTRACT. Fatigue cracks are common and potentially critical defects in metallic plate-like structures, and ultrasonic guided wave methods provide an efficient and relatively low-cost means of crack detection and monitoring. However, widely used baseline subtraction methods may fail under mismatched environmental and operational conditions. In particular, varying applied loads change not only the contact state of a crack but also specimen dimensions and wave speeds, which affect the ultrasonic signal response. The load dependence of crack opening provides a possibility for enhanced crack detection, which is well-known for higher frequency bulk waves. A load-differential method is proposed in this paper whereby guided wave signals obtained at different loads under the same damage state are compared without utilizing previously recorded damage-free data. To demonstrate this method, a fatigue test was performed on an aluminum plate specimen instrumented with a sparse array of piezoelectric transducers. Signal changes due to crack opening effects caused by increasing tensile loads are visualized using delay-and-sum imaging. The results show that the load-differential method is capable of detecting cracks and visualizing their locations.

Keywords: Guided Wave, Sparse Array, Load-differential Imaging, Crack Detection

Approved for public release; distribution unlimited

1. INTRODUCTION

Compared to current nondestructive evaluation (NDE) approaches, structural health monitoring (SHM) methods are widely regarded as being able to significantly reduce inspection time and cost. For plate-like structures, an SHM system based on Lamb wave propagation offers promise for damage detection because of the ability of such waves to travel long distances with low amplitude damping [1-3]. Research on sensor array design and signal processing as applied to this approach has been undertaken within recent years, and indicates both its promise and pitfalls.

Different sensor array geometries have been proposed to implement guided wave NDE and SHM systems. Zhao *et al.* [4] compared circular, rectangular and parallel linear arrays for Lamb wave tomography. Yu and Giurgiutiu [5] constructed five different 2-D compact phased arrays and applied beamforming to compare the angular range for damage detection of the five geometries. One limitation of the above array geometries is the requirement of a relatively large number of transducers. A sparse (i.e., spatially distributed) array geometry was introduced by Wang *et al.* [6] and later used by Michaels *et al.* [7] and others to achieve detection and localization of discrete damage using fewer transducers than are required for tomographic and compact array approaches. Another advantage of the sparse array geometry is that forward scattered as well as backscattered signals are incorporated into imaging algorithms.

The idea of baseline comparison plays a key role in many SHM methods. Ideally, by subtracting baseline signals recorded from the damage free structure from current test signals, a residual signal, which is assumed to arise from damage, is obtained. A variety of signal processing algorithms can be applied to these residual signals for damage detection, localization and

Approved for public release; distribution unlimited

characterization. However, such a process is strongly affected by mismatched environmental and operational conditions. Lu and Michaels [8] and Konstantinidis *et al.* [9] both addressed the temperature mismatch problem by optimal baseline selection, where a number of baselines were recorded at different temperatures and the optimal baseline that minimized the residual signal was selected. Lu and Michaels [8] originally proposed the signal stretch method applied to the optimal baseline to further match the current test signals, which has since been used by others.

Another environmental condition, surface wetting, was investigated with a carefully designed experiment by Lu and Michaels [10]. Different features extracted from diffuse ultrasonic wave signals were evaluated for damage detection in the presence of surface wetting and all features were shown to have some capability of discriminating surface wetting from damage. Li *et al.* [11] recently studied the effects that surface wetting can have on guided waves and results indicate that guided wave SHM systems cannot perform properly if there are even small changes in surface wetting.

The effects of loads on properties of guided waves in cable and rail structures were investigated via a finite element method by Chen and Wilcox [12]. Michaels *et al.* [13] examined the effects of applied uniaxial loads on both the short-time and long-time guided wave signals and showed damage detection methods that rely upon signal changes such as most damage indices were likely to fail in the presence of loading variations.

Fatigue cracks are one of the most common defect types in metallic plate structures and normally initiate from fastener holes. Notches are commonly used to simulate cracks, and a number of

Approved for public release; distribution unlimited

studies have been reported on the interactions of guided waves with notches and cracks [1,14,15]. One of major differences between the two interactions is the load dependence of crack closure. It is well known that closed cracks are hard to detect with conventional ultrasonic testing methods because ultrasound can propagate through a tightly closed crack [16,17]. Research on load modulation of ultrasound with fatigue cracks can be traced back to 1970s and has been the subject of a number of investigations. Frandsen *et al.* [16] used acoustic techniques to qualitatively measure the area over which closure occurred. Kim *et al.* [18] investigated closed fatigue cracks using surface acoustic waves and suggested that modulation of loading about a low mean static load was able to enhance the detection of small closed cracks. Mi *et al.* [19] used the bulk wave energy transmitted through the region of a fastener hole to dynamically monitor the initiation and growth of fatigue cracks. Ohara *et al.* [20] recently introduced a nonlinear ultrasonic imaging method whereby a phased array was used to create linear and subharmonic images. Images obtained at different applied loads were subtracted to better visualize fatigue cracks.

This paper builds upon previous work by the authors [21-23] in which the basic delay-and-sum imaging method is applied in conjunction with varying external loads. In contrast to the work described in [20], signals rather than images are differenced, and these differenced signals are used for detection and localization of fatigue cracks. By calculating residual signals at varying loads at the same state of damage, fatigue cracks can be assessed without requiring baseline data recorded from the undamaged specimen.

Approved for public release; distribution unlimited

The paper is organized as follows: Section 2 describes the fatigue testing protocol. Section 3 reviews the delay-and-sum imaging algorithm. Section 4 discusses the effects of applied loads on baseline subtraction imaging. Section 5 introduces the load-differential method and demonstrates performance on fatigue test data, and Section 6 contains the concluding remarks.

2. EXPERIMENT

Fatigue cracks were initiated and grown in a 6061-T6 aluminum alloy plate of dimensions 305 mm × 610 mm × 3.18 mm. As can be seen in Figure 1(a), an array of six piezoelectric transducers was affixed to one side of the plate using two-component epoxy, and each transducer was further backed with a bubble-filled epoxy protection layer. The surface mounted transducers were fabricated from 300 kHz, radial mode PZT discs (7 mm in diameter and 0.5 mm thick).

The aluminum specimen was then mounted in a servo-hydraulic test machine running in load control mode as shown in Figure 1(b). A National Instrument PXIe-5122 waveform generator was used to generate a liner chirp excitation sweeping from 50 to 500 kHz with a duration of 0.2 ms. A Panametrics 5072PR pulser-receiver was used to amplify the received signals and a custom multiplexer switched between the 15 unique transmit-receive pairs. The received signals were then digitized by a National Instrument PXI-5412 14-bit digitizer at a sampling frequency of 20 MHz. For each acquisition, 20 waveforms were averaged to improve the signal-to-noise ratio.

The broadband chirp excitation resulted in multiple Lamb wave modes propagating in the plate. Received signals were filtered to yield the equivalent narrow-band tone burst response as

Approved for public release; distribution unlimited

described in [24]. A 3-cycle Hanning windowed tone burst response centered at 100 kHz was selected because of the purity of the A_0 mode and its sensitivity to through-thickness cracks.

Prior to fatiguing the specimen, a set of baseline signals was recorded from the pristine sample. A through hole measuring 5.1 mm in diameter was then drilled in the center of the plate, and a small starter notch was introduced on the left side of the hole as a crack initiator. The plate was fatigued with a 3 Hz sinusoidal tension-tension load ranging from 16.5 to 165 MPa. Fatiguing was periodically paused and ultrasonic data were recorded as a function of applied static tensile load from 0 to 115 MPa in steps of 11.5 MPa, which corresponds to 0% to 100% load with a 10% load step (11 loading conditions for each data set). Fatiguing was continued until the largest crack was about 25 mm in length. Fatigue cycles and observations of the cracks are summarized in Table 1 for each data set.

3. ANALYSIS METHODOLOGY

Guided wave imaging algorithms are used to visualize information obtained from the transducer arrays. The basic delay-and sum imaging method for sparse arrays was introduced by Wang *et al.* [6], where each image pixel value was calculated as the summation of the residual signals (current signals minus baselines) at different points in time. This method has subsequently been used by other researchers to locate various types of damage in plate-like structures [7,25].

The basic delay-and-sum imaging method is reviewed here. Consider two sets of data recorded from all transducer pairs of a sparse array at different times. These two different times could correspond to before and after introduction of damage, or before and after a change in environmental or operational conditions. The 15-signal set recorded at the first time is referred to

Approved for public release; distribution unlimited

as the reference signals and the set recorded later as the current signals. Now consider sensor pair *ij* where the *i*th transducer (the transmitter) is located at (x_i,y_i), and the *j*th transducer (the receiver) is located at (x_j,y_j). If a scatterer is introduced at location (x,y), the delay time, which corresponds to the time of the wave propagating from the transmitter to the receiver by way of the scatterer, is:

$$t_{xy}^{ij} = \frac{\sqrt{(x_i - x)^2 + (y_i - y)^2} + \sqrt{(x_j - x)^2 + (y_j - y)^2}}{c_g}, \tag{1}$$

where c_g is the group velocity. Let $s_{ij}(t)$ refer to the differenced signal computed by subtraction of the reference signal from the current signal for sensor pair *ij*. The signal $s_{xy}(t)$ is calculated as the sum of the differenced signals delayed by the appropriate time shifts resulting from the scattering path going through the point (x,y):

$$s_{xy}(t) = \sum_i \sum_j s_{ij}(t - t_{xy}^{ij}). \tag{2}$$

The image value at pixel (x,y) is:

$$E_{xy} = \int_{t_1}^{t_2} s_{xy}^2(t)dt, \tag{3}$$

where t_1 and t_2 are the start and end times of the selected time window. Although the differenced signal in Eq. (3) can be either the raw (RF) signal or the envelope-detected (rectified) signal, here we only consider the envelope-detected signals. The group velocity c_g is estimated from the arrival times of the direct waves propagating between all transducer pairs as described in [7]. Values for t_1 and t_2 are calculated to yield a very narrow time window centered at the nominal peak of the scattered arrival.

Approved for public release; distribution unlimited

4. IMAGING WITH DAMAGE-FREE BASELINES

The imaging algorithm is first applied to residual signals computed from damage-free baseline signals. Consider images constructed from data set 2 (current signals) and data set 1 (damage-free baseline signals), between which the only difference is drilling of the 5 mm center hole. Figure 2 shows three images that were generated from current signals and baselines recorded at identical loads. At the matched loads of 0%, 50% and 100%, the three images are almost identical because the static load has minimal effects on the through-hole.

The results are much different when the same imaging algorithm is applied to the data sets under mismatched loads. Figure 3 shows three images also constructed between data sets 1 and 2, where the baselines were recorded at zero load and the current signals were recorded at 20%, 60% and 100% loads. Although there is a 20% load mismatch for Figure 3(a), the image is not significantly degraded as compared to the images of Figure 2 and the center hole is clearly observed. However, as the load mismatch increases, the image with a 60% load mismatch is obviously degraded as Figure 3(b) shows. The image of Figure 3(c) with a 100% load mismatch is degraded to a degree that the hole is no longer detectable.

Image degradation under mismatched loads is explained by considering the effects of applied loads on guided wave propagation. There are two primary effects: (1) specimen dimension changes, and (2) guided wave speed changes due to the acoustoelastic effect [26]. Both of these changes perturb the time of arrival of individual echoes, and thus result in significant residual signals from baseline subtractions regardless of whether damage has also been introduced.

Approved for public release; distribution unlimited

Now consider images obtained from data set 7 (current signals) and data set 3 (baseline signals), where the primary difference between the two data sets is a 5.4 mm long single crack. Unlike Figure 2, which illustrates that matched applied loads have only very small effects on the through-hole, Figure 4 shows the much more significant effects that applied loads can have on a fatigue crack. As shown in Figure 4(a), the crack is not detectable at zero load because it is still tightly closed. By increasing the applied load, clear crack detection is obtained as the crack opens. Figure 4(b) is generated at 60% load and Figure 4(c) is generated at 100% load, and it is obvious that higher loads open the crack more completely and thus the images are improved.

Figure 5 shows the images of data set 3 and data set 7 under mismatched loads where current signals were all recorded at 0% load but baseline signals were recorded at 20%, 60% and 100% loads. The crack is closed at zero load and thus the guided waves propagate through it with almost no measurable effect. This situation produces images that are essentially identical to those that would be obtained if there were no damage and illustrate the effects of applied loads only. These images show that the mismatched loads generate stronger artifacts around the image edges; however, the residual signal energy from these artifacts in Figure 5(c) is about 3dB less than that from the opened crack shown in Figure 4(c).

Figure 6 shows the images of data set 3 and date set 7 under mismatched loads where current signals were recorded at 100% load and baseline signals were recorded at 0%, 40% and 80% loads. As shown in Figures 6(a) and 6(b), the crack is not detected when the loads are significantly mismatched even though it is fully opened. The image of Figure 6(c), which has only a 20% load mismatch, clearly shows the crack and is not significantly degraded from

Approved for public release; distribution unlimited

Figure 4(c). These results, along with those shown in Figure 3(a) for the hole, indicate that load mismatches of up to 20% (23 MPa) can be tolerated.

5. LOAD-DIFFERENTIAL IMAGING

The results of the previous section motivate an alternative approach for fatigue crack detection and localization – load-differential imaging. For this method signals recorded at one load are referred to as the "baseline signals", and the signals recorded at the same damage state but at a slightly increased tensile load are called the "current signals". Differences between the signals are thus caused by a combination of crack opening effects and loading effects. Figures 3(a) and 6(c) indicate that a 20% load difference (or less) will not adversely affect imaging of damage. To minimize artifacts resulting from loading while maintaining detection, a 10% load difference is selected. Baseline loads start from 0% and end at 90% with a increment of 10%, and the current signal loads range from 10% to 100% accordingly; a total of 10 differential-load pairs are thus considered for each data set.

5.1 Pair-wise load-differential signals

Figure 7 shows received signals at 11 loads from two transducer pairs of data set 10, where two cracks are present. Signals for each transducer pair are normalized by the peak amplitude of the first arrival at 0% load, where cracks are assumed to be less opened or possibly even closed. Figure 7(a) shows signals from transducer pair 2-5 (i.e., transmitting on 2 and receiving on 5), where the incident wave is broadside to the cracks and received signals are thus strongly affected by opening of the cracks with load. There is an abrupt amplitude drop between 0% load and 10% load within the time window of the first arrival of A_0 mode, which is between 80 and

Approved for public release; distribution unlimited

110 us. The signals amplitude continues to decrease as loads increase and further open the cracks. Figure 7(b) shows signals from the transducer pair 1-3, where the direct path does not go through the cracked area and thus the signals are less affected by the cracks. The signal amplitude and shape change with load between 90 and 120 us, which corresponds to the path of propagation from the transmitter to the cracks to the receiver.

Figure 8 shows waterfall plots of the ten load-differential signals for transducer pairs 2-5 and 1-3, where signals are normalized as previously described prior to subtraction. Figure 8(a) shows more clearly that the larger crack on one side of the hole opens up and blocks the transmitting guided wave, resulting in the large amplitude change of the first arrival. At about 70% load the smaller crack on the other side opens up and decreases the signal amplitude further. For Figure 8(b), the residual signals correspond to guided waves reflected from the crack site. Similar effects can be observed as one crack opens at lower load and another crack opens at higher load.

5.2 Load-differential images

Load-differential signals such as shown in Figure 8 can be used as the differenced signals in Eq. (2) to generate ten load-differential images for each data set, which correspond to differential loads ranging from 0-10% to 90-100%. Figure 9 is the image collage constructed from all 14 data sets recorded from the fatigue test. All images from the first four data sets are very similar because there are no cracks even though there are changes to the specimen (i.e., introduction of the drilled hole and starter notch). The first crack is barely seen at 40% load from the images of data set 6, and is clearly visible at data set 7. From data set 7 to data set 9, images that show the

Approved for public release; distribution unlimited

crack appear at progressively lower loads, which is consistent with the crack growing as fatiguing continues and thus becoming easier to open at lower loads. For data set 10, the crack on one side of the hole starts to open at very low loads (0-10% load), whereas the crack on the other side of the hole opens up at higher loads (50-60% load); both cracks are completely opened at 90% load. Images from data sets 11-14 continue to show that the cracks become easier to open at low loads as both cracks keep growing. By data set 14 both cracks are very large, but there is still some evidence that they are not opening simultaneously.

The images are also capable of discriminating between the two cracks on either side of the hole. Figure 10 shows three images from data 12 at 20-30% load, 30-40% load, and 60-70% load, respectively. Figure 10(a) clearly shows that one crack on the left side of the hole opens up at 30% load. At 40% load, as shown in Figure 10(b), the left side crack is almost fully opened and the crack on the right side of the hole starts to open up. Finally, as can be seen in Figure 10(c), at 70% load the right side is also fully opened.

6. SUMMARY AND CONCLUSIONS

This paper has investigated the positive and negative effects of loads on ultrasonic guided wave imaging systems that are based upon changes from damage-free baselines. A large mismatched load can cause significant changes in ultrasonic signals and can thus result in both false alarms and missed detection of damage. However, a relatively small load can open cracks to enhance their detectability. These observations have motivated the introduction and demonstration of a load-differential imaging method for fatigue crack detection and localization. A series of images generated from load-differential signals clearly show the initiation and progression of fatigue

Approved for public release; distribution unlimited

crack growth. Furthermore, load-differential imaging has the potential for identifying multiple cracks if they open at different loads.

Load-differential methods clearly demonstrate the importance of having open cracks to ensure their reliable detection. Although temperature was nominally constant for the data shown here, it should be noted that temperature or other environmental conditions will not adversely affect load-differential imaging performance as long as there are not significant changes in between load steps. Future work remains in exploring advanced imaging algorithms, testing with more complicated sample geometries, and assessing the ability to distinguish benign loading effects from damage.

ACKNOWLEDGEMENTS

The authors gratefully acknowledge and appreciate the support of the Air Force Research Laboratory under Contract No. FA8650-09-C-5206 (Charles Buynak, Program Manager).

REFERENCES

1. D. N. Alleyne and P. Cawley, "The interaction of Lamb waves with defects," *IEEE Transactions on Ultrasonics, Ferrolectrics, and Frequency Control*, **39**(3), pp. 381-397, 1992.

2. J. L. Rose, "A baseline and vision of ultrasonic guided wave inspection potential," *Journal of Pressure Vessel Technology*, **124**, pp. 273-282, 2002.

3. A. Raghavan and C. E. S. Cesnik, "Review of Guided-wave Structural Health Monitoring," *The Shock and Vibration Digest,* **39**(2), pp. 91-114, 2007.

4. X. Zhao, R. L Royer, S. E. Owens and J. L. Rose, "Ultrasonic Lamb wave tomography in structural health monitoring," *Smart Materials and Structures*. **20**, 105002, 2011.

Approved for public release; distribution unlimited

5. L. Yu and V. Giurgiutiu, "In situ 2-D piezoelectric wafer active sensors arrays for guided wave damage detection," *Ultrasonics*, **48**, pp. 117-134, 2008.

6. C. H. Wang, J. T. Rose, and F.-K. Chang, "A synthetic time-reversal imaging method for structural health monitoring," *Smart Materials and Structures*, **13**(2), pp. 415-423, 2004.

7. J. E. Michaels, "Detection, localization and characterization of damage in plates with an *in situ* array of spatially distributed ultrasonic sensors," *Smart Materials and Structures*, **17**, No. 035035 (15pp), 2008.

8. Y. Lu and J. E. Michaels, "A methodology for structural health monitoring with diffuse ultrasonic waves in the presence of temperature variations," *Ultrasonics*, **43**, pp. 717-731, 2005.

9. G. Konstantinidis, B. W. Drinkwater, and P. D. Wilcox, "The temperature stability of guided wave structural health monitoring systems," *Smart Material and Structures*, **15**(4), pp. 967-976, 2006.

10. Y. Lu and J. E. Michaels, "Feature extraction and sensor fusion for ultrasonic structural health monitoring under changing environmental conditions," *IEEE Sensors Journal*, **9**(11), pp. 1462-1471, 2009.

11. H. Li, J. E. Michaels, S. J. Lee, and T. E. Michaels, "Quantification of surface wetting in plate-like structures via guided waves," in *Review of Progress in QNDE*, **31**, in press, expected 2012.

12. F. Chen and P. D. Wilcox, "The effect of load on guided wave propagation," *Ultrasonics*, **47**, pp.111-122, 2007.

13. J. E. Michaels, S. J. Lee and T. E. Michaels, "Impact of applied loads on guided wave structural health monitoring," *in Review of Progress in QNDE*, **30**, pp. 1515-1522, 2011.

14. Y. Cho, D. Hongerholt, and J. Rose, "Lamb wave scattering analysis for reflector characterization," *IEEE Transactions on Ultrasonics, Ferrolectrics, and Frequency Control*, **44**, pp. 44–52, 1997.

15. M. J. S. Lowe, P. Cawley, J. Y. Kao and O. Diligent, "The low frequency reflection characteristics of the fundamental antisymmetric Lamb wave a0 from a rectangular notch in a plate." *Journal of the Acoustical Society of America*, **112**(6), pp. 2612-2622, 2002.

16. J. D. Frandsen, R. V. Inman, and O. Buck, "Comparison of acoustic and strain gauge techniques for crack closure," *International Journal of Fracture*, **11**, pp. 345–348, 1975.

17. S. J. Bowles, C. A. Harding, and G. R. Hugo, "Effect of crack closure on ultrasonic detection of fatigue cracks at fastener holes," *American Institute of Physics Conference Proceedings*, **1096**, pp.1878-1885, 2009.

Approved for public release; distribution unlimited

18. J. Y. Kim, V. A. Yakovlev, and S. I. Rokhlin, "Surface acoustic wave modulation on a partially closed fatigue crack," Journal of the Acoustical Society of America, **115**, pp. 1961–1972, 2004.

19. B. Mi, J. E. Michaels and T. E. Michaels, "An ultrasonic method for dynamic monitoring of fatigue crack initiation and growth," *Journal of the Acoustical Society of America*, **119**(1), pp. 74-85, 2005.

20. Y. Ohara, S. Horinouchi, M. Hashimoto, Y. Shintaku, and K. Yamanaka, "Nonlinear ultrasonic imaging method for closed cracks using subtraction of responses at different external loads," *Ultrasonics*, **51**, pp.661-666, 2011.

21. J. E. Michaels, S. J. Lee, X. Chen and T. E. Michaels, "Load-enhanced imaging of fatigue cracks via sparse guided wave arrays," *Proceedings of the 8th International Workshop on Structural Health Monitoring*, pp. 1150-1157, 2011.

22. J. E. Michaels, S. J. Lee, X. Chen, F. Shi and T. E. Michaels, "Understanding and exploiting applied loads for guided wave structural health monitoring," *2011 Aircraft Airworthiness & Sustainment Conference*, San Diego, CA, April 18-21, 2011.

23. S. J. Lee, J. E. Michaels, X. Chen and T. E. Michaels, "Fatigue crack monitoring via load-differential guided wave methods," *Review of Progress in Quantitative Nondestructive Evaluation*, **31**, in press, expected 2012.

24. J. E. Michaels, S. J. Lee, J. S. Hall, and T. E. Michaels, "Multi-mode and multi-frequency guided wave imaging via chirp excitations," *Proceedings of SPIE*, **7984**, edited by T. Kundu, 79840I (11 pp), 2011.

25. T. Clarke, P. Cawley. P. D. Wilcox and A. J. Croxford, " Evaluation of the damage detection capability of a sparse-array guided-wave SHM system applied to a complex structure under varying thermal conditions, " *IEEE Transactions on Ultrasonics, Ferrolectrics, and Frequency Control*, **56**(12), pp. 2666-2678, 2009.

26. N. Gandhi, J. E. Michaels and S. J. Lee, "Acoustoelastic Lamb wave propagation in a homogeneous, isotropic aluminum plate," *in Review of Progress in QNDE*, **30**, pp. 161-168, 2011.

Approved for public release; distribution unlimited

Table 1. Summary of Recorded Data, Fatiguing Schedule, and Observations

Data Set	Fatigue Cycles	Notes / Crack Lengths at Surface	
		Left	Right
1	0	Baseline, no hole, no notch	
2	0	5.1 mm diameter hole drilled	
3	0	Starter notch cut (left, front of hole)	
4	5,000	No visible cracks	
5	8,000	1.6 mm	----
6	10,000	3.6 mm	----
7	12,500	5.4 mm	----
8	15,500	7.7 mm	----
9	17,000	9.9 mm	----
10	18,500	13.4 mm	4.7 mm
11	19,500	16.8 mm	8.4 mm
12	20,000	19.5 mm	11.5 mm
13	20,400	22.7 mm	15.6 mm
14	20,600	25.2 mm	18.8 mm

Approved for public release; distribution unlimited

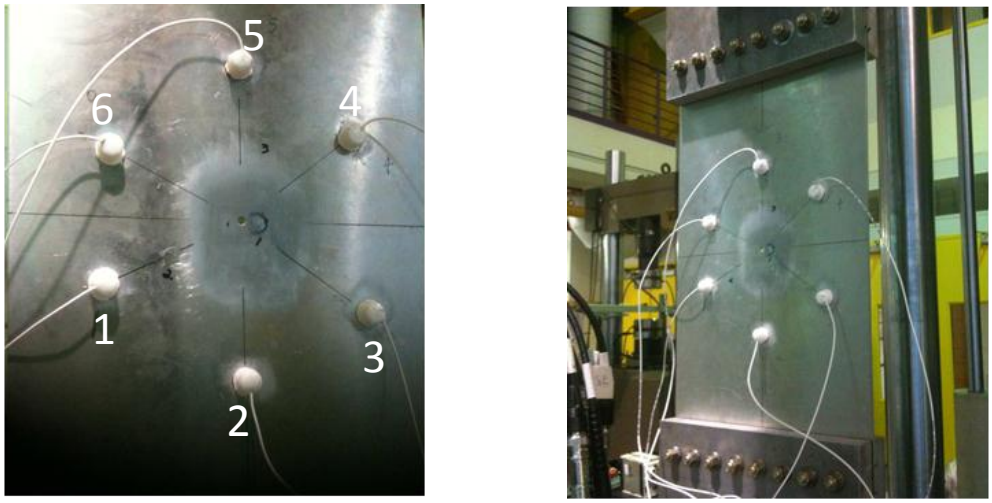

(a) (b)

Figure 1. Aluminum plate mounted in the MTS machine prior to fatiguing.

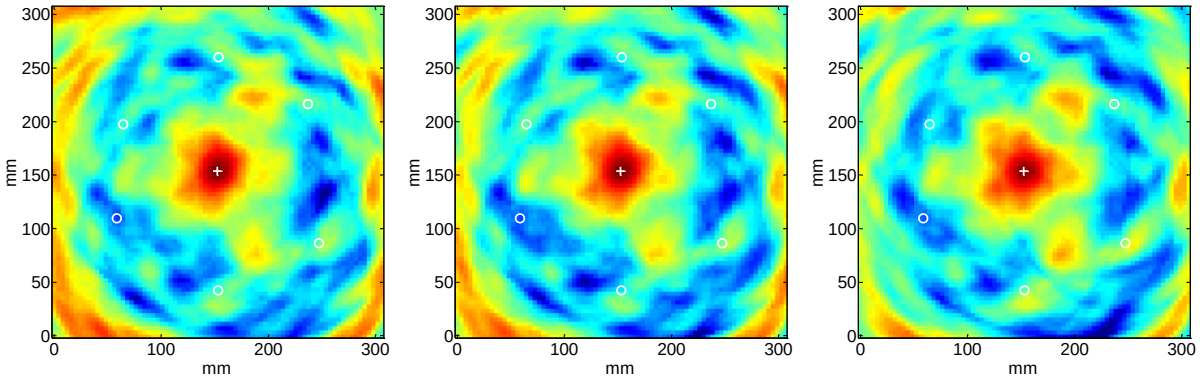

(a) (b) (c)

Figure 2. Images generated between data set 1 (baseline signals) and data set 2 (current signals, after hole drilled) at matched loads. (a) 0 MPa (0% load), (b) 57.5 MPa (50% load), and (c) 115 MPa (100% load). All three images are shown on the same 10 dB color scale (-55 dB to -65 dB).

Approved for public release; distribution unlimited

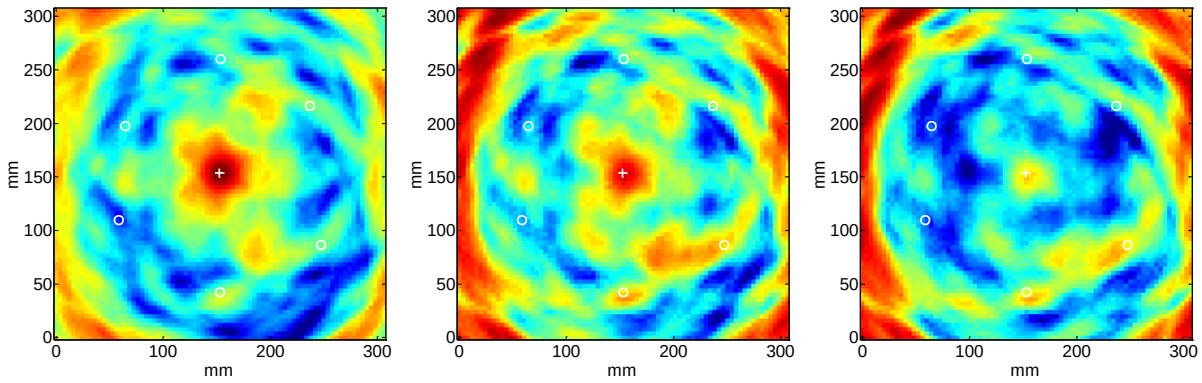

(a) (b) (c)

Figure 3. Images generated between data set 1 (baseline signals) and data set 2 (current signals, after hole drilled) at mismatched loads. All three images are shown on a 10 dB color scale normalized to their maximum amplitudes. (a) 0/23 MPa (0/20% load), max amplitude of -55 dB, (b) 0/69 MPa (0/60% load), max amplitude of -54 dB, and (c) 0/115 MPa (0/100% load), max amplitude of -50 dB.

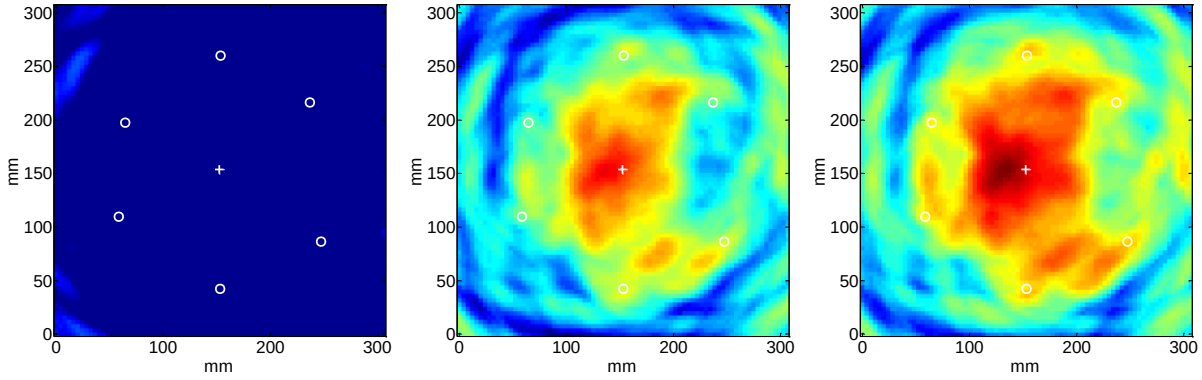

(a) (b) (c)

Figure 4. Images generated between data set 3 (baseline signals) and data set 7 (current signals, 5.4 mm long fatigue crack) at matched loads. (a) 0 MPa (0% load), (b) 57.5 MPa (50% load), and (c) 115 MPa (100% load). All three images are shown on the same 10 dB color scale (-58 dB to -48 dB).

Approved for public release; distribution unlimited

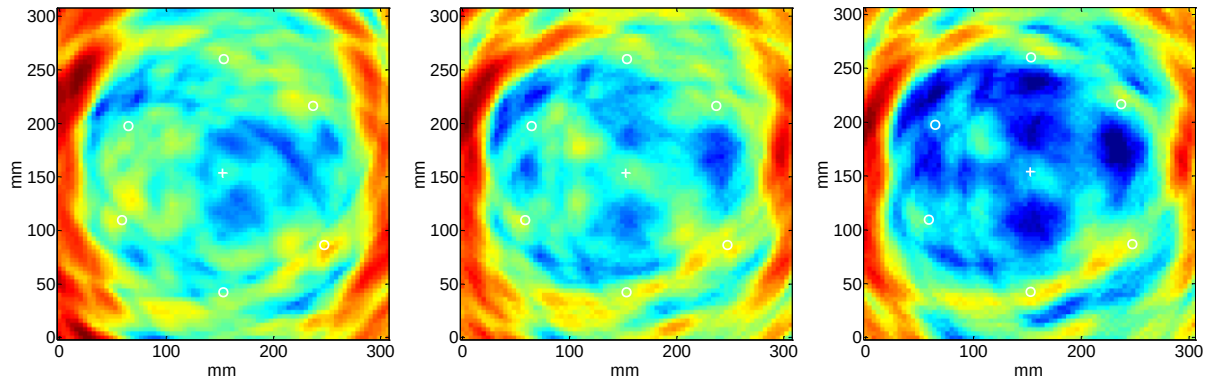

(a) (b) (c)

Figure 5. Images generated between data set 3 (baseline signals) and data set 7 (current signals, 5.4 mm long fatigue crack) at mismatched loads. All three images are shown on a 10 dB color scale normalized to their maximum amplitudes. (a) 23/0 MPa (20/0% load), max amplitude of -57 dB, (b) 69/0 MPa (60/0% load), max amplitude of -55 dB, and (c) 115/0 MPa (100/0% load), max amplitude of -51 dB.

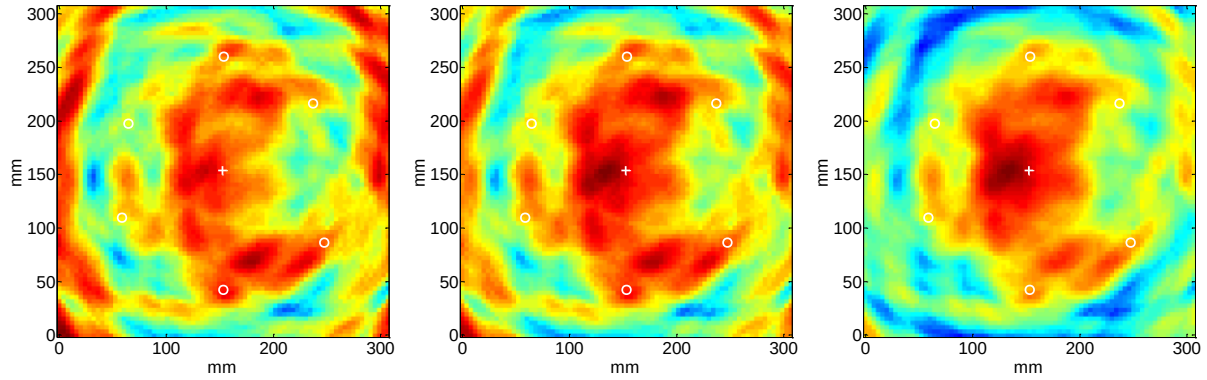

(a) (b) (c)

Figure 6. Images generated between data set 3 (baseline signals) and data set 7 (current signals, 5.4 mm long fatigue crack) at mismatched loads. All three images are shown on a 10 dB color scale normalized to their maximum amplitudes. (a) 0/115 MPa (0/100% load), max amplitude of -48 dB, (b) 46/115 MPa (40/100% load), max amplitude of -49 dB, and (c) 92/115 MPa (80/100% load), max amplitude of -49 dB.

Approved for public release; distribution unlimited

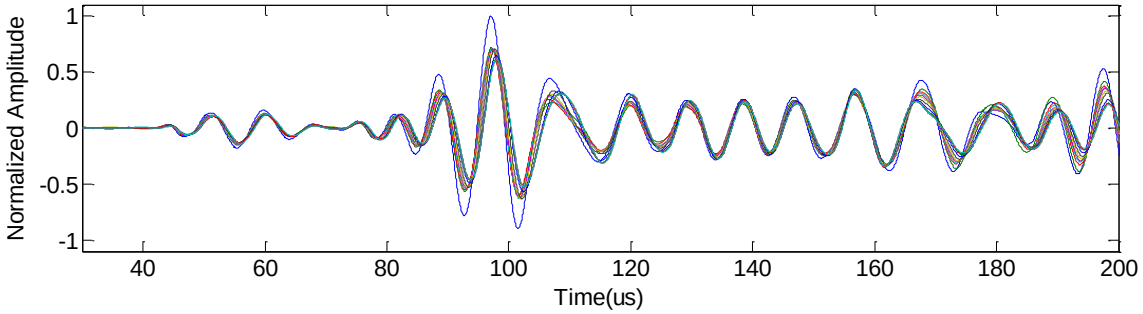

(a)

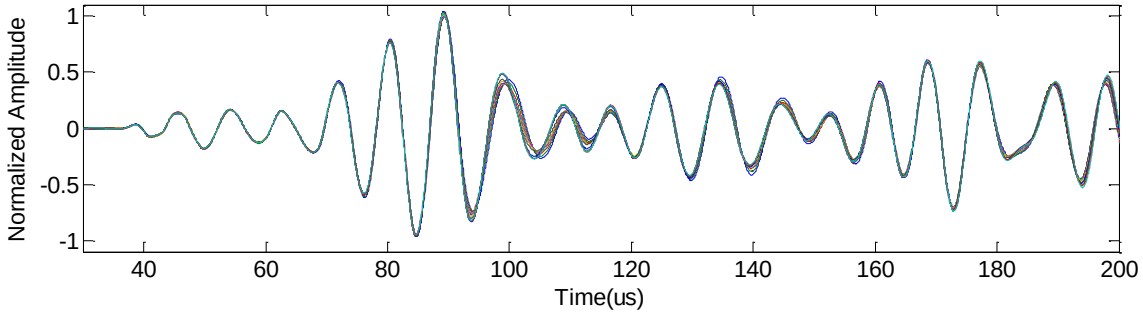

(b)

Figure 7. Signals recorded from data set 10 at 11 loads ranging from 0 to 115 MPa (0 to 100%). (a) Transducer pair 2-5, and (b) transducer pair 1-3.

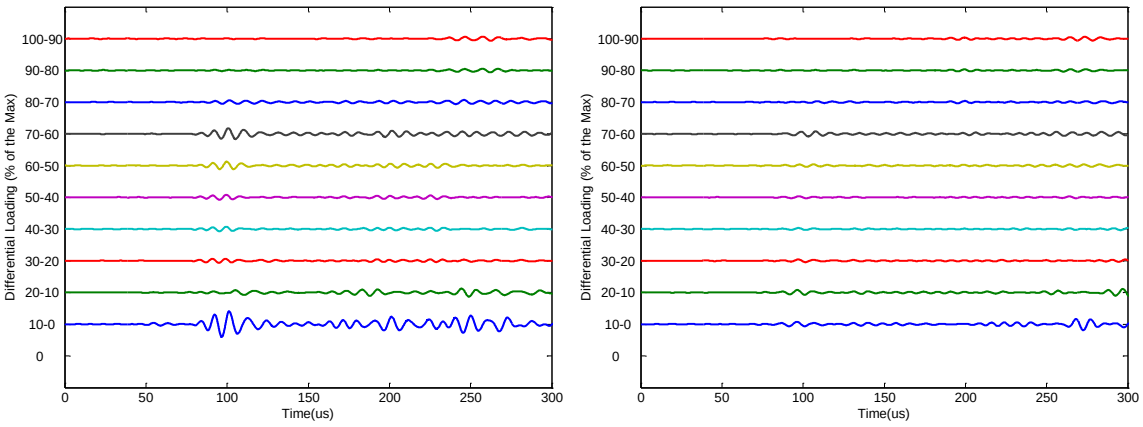

(a) (b)

Figure 8. Differential signals from data set 10 at ten differential loads (0-to-10%, 10-to-20%, … 90-100%). (a) Transducer pair 2-5, and (b) Transducer pair 1-3.

Approved for public release; distribution unlimited

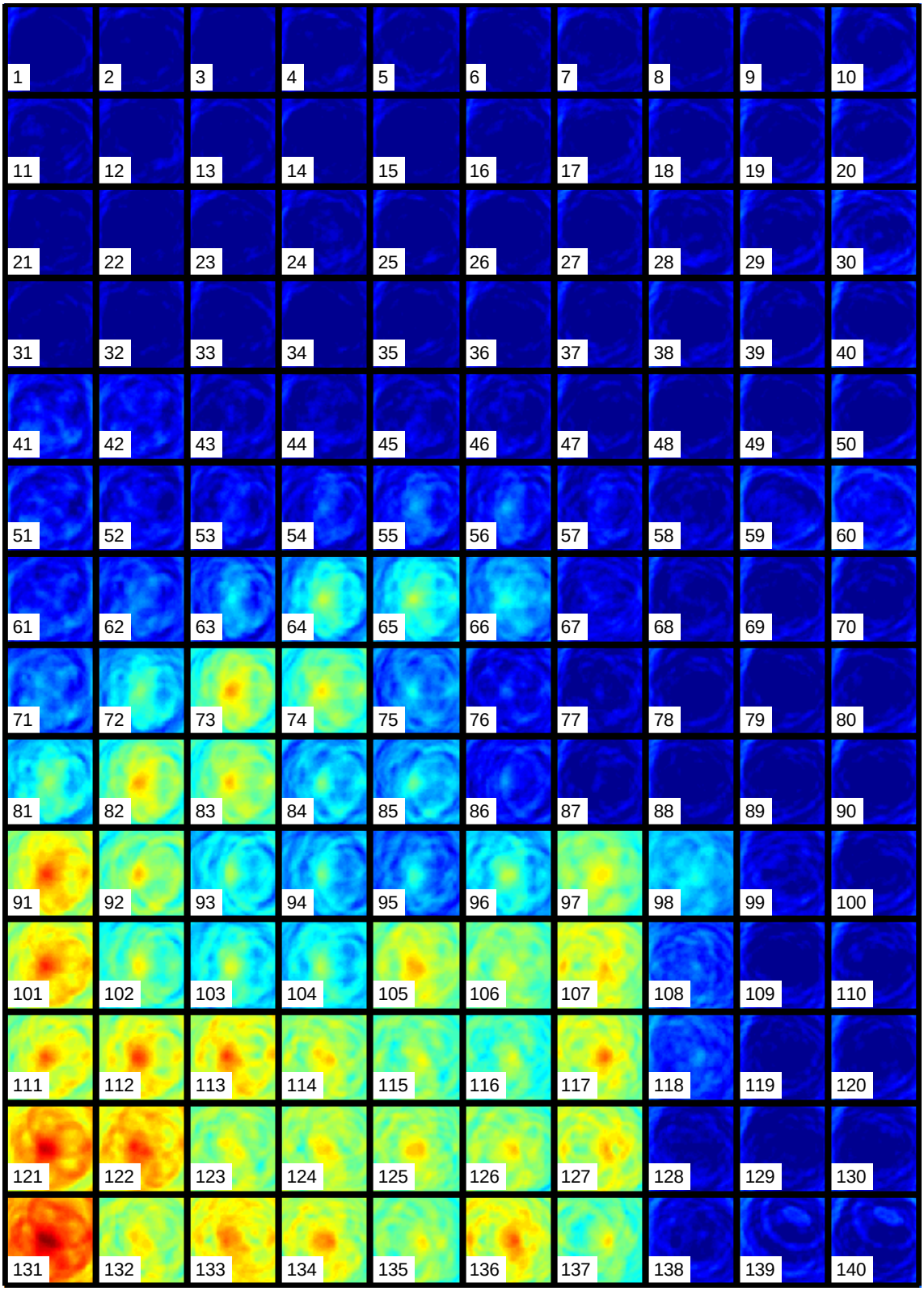

Figure 9. Load-differential images of all 14 data sets plotted on a fixed 30 dB scale (-63 dB to -33 dB).

Approved for public release; distribution unlimited

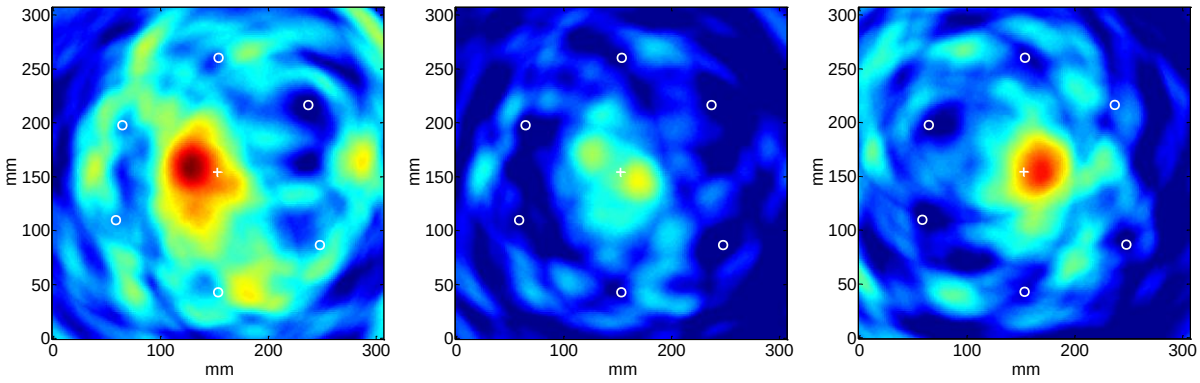

(a) (b) (c)

Figure 10. Load-differential images generated from data set 12. (a) 23/34.5 MPa (20/30%), (b) 34.5/46 MPa (30/40%), and (c) 69/80.5 MPa (60/70%). All three images are shown on the same 10 dB color scale (-60 dB to -50 dB).

Approved for public release; distribution unlimited